RSC Advances

PAPER

View Article Online
View Journal | View Issue

Cite this: *RSC Adv.*, 2017, **7**, 39539

Ag nanoparticles supported on nickel foam: a flexible 3D electrode for methanol electrocatalytic oxidation†

Yanan Yu,[a] Yu Cheng,[a] Meisong Guo,[a] Chenzhong Li[c] and Jingbo Hu *[ab]

Ag nanoparticles (NPs) were prepared on nickel foam (NF) electrode coated Nafion membranes (N-AgNPs/NF) using an ion-implantation method. NF is a flexible 3D electrode. The influence of the supporting material on both the morphology and the electrocatalytic activity of AgNPs for the electrocatalytic oxidation of methanol are investigated and compared with AgNPs on an indium tin oxide electrode (AgNPs/ITO). Scanning electron microscopy (SEM) data indicated that spherical monodispersed NPs were obtained on NF and ITO substrates with a size distribution in the range of 10 to 20 nm and 3 to 6 nm, respectively. The influence of the support material on the electrocatalytic activity is tested by means of cyclic voltammetry (CV) for the electrocatalytic oxidation of methanol in alkaline electrolytes. The N-AgNPs/NF electrode exhibited greater electrocatalytic activity than the AgNPs/ITO electrode for the electrocatalytic oxidation of methanol. Beneficial electrocatalytic activity is measured due to the interplay between support and AgNPs. The N-AgNPs/NF electrode has long-term stability for the electrocatalytic oxidation of methanol and possible applications in fuel cells.

Received 14th June 2017
Accepted 7th August 2017

DOI: 10.1039/c7ra06656b

rsc.li/rsc-advances

1 Introduction

Highly flexible and wearable devices have benefit for modern life in various fields such as robotic sensory skins, roll-up displays, mobile gadgets, and biomedical devices.[1–5] Accordingly, continuous advances in flexible energy storage devices such as lithium-ion batteries,[6] supercapacitors,[7,8] and fuel cells[9,10] are required to autonomously operate wearable and portable device systems. To date, versatile and flexible electrode materials including carbon textile, carbon fiber, and carbon nanotube coated cotton paper substrates have been used in electrochemical study owing to their good flexibility, light weight, good sustainability, and foldable nature.[11–13] However, they are somewhat expensive, and a relatively complicated fabrication process would be required to manufacture these substrates which may impede their practical applications in wearable energy storage devices. In this respect, it is desirable to attempt to utilize cost-effective nickel foam (NF) substrate as a multifunctional substrate.

Nickel foam has been commercially available for over two decades due to its good electrocatalytic activity, large specific surface area, high porosity that favors reactant mass transfer, good mechanical strength, electrical conductivity and corrosion resistance.[14–17] In order to enhance the catalytic activity of Ni, several groups investigated the modification method of NF by deposition of noble metals and other chemicals, with the aim of producing electrodes for fuel cells,[18–20] water electrolyzers,[21,22] hydrogen storage,[23,24] and degradation of pollutants.[25,26]

Silver nanoparticles (AgNPs) have attracted extensive interest due to its unique shape, properties and have applied to gigantic range of applications as substrates for catalysis, antibiosis and sensing,[27–29] especially the development on electrocatalytic oxidation of methanol in recent years.[30–32] Assembling silver on supports can not only endow AgNPs with high activity but also facilitate the operation while fabricating a much smaller active component. AgNPs could be located on various supports including NF, and the resulting systems exhibit preeminent performance in diversified applications.[33–35] NF supported metal nanomaterials including silver have applied as a modified electrode towards electrocatalytic oxidation of small organic molecules. To effectively deposit noble metal nanoparticles into the 3D structure support, two main strategies were employed: spontaneous deposition[36,37] and electrodeposition.[38,39] However, most preparation methods are difficult to operate, and control the size of the particles during fabrication. Ion implantation is a type of material surface modification technique that provides practical and excellent electrode materials with long-term stability.

[a]College of Chemistry, Beijing Normal University, Beijing 100875, PR China. E-mail: hujingbo@bnu.edu.cn

[b]Key Laboratory of Beam Technology, Material Modification of Ministry of Education, Beijing Normal University, Beijing 100875, PR China

[c]Nanobioengineering/Nanobioelectronics Laboratory, Department of Biomedical Engineering, Florida International University, 10555 West Flagler Street, Miami, FL 33174, USA

† Electronic supplementary information (ESI) available. See DOI: 10.1039/c7ra06656b

Direct methanol fuel cells (DMFCs), which employ renewable and easy-handling methanol as a green fuel and offer a theoretical energy density as high as 4.8 kW h L^{-1}, have attracted increasing attention in recent decade as a promising power sources.[40–42]

Herein, we have successfully fabricated the novel Ag nanoparticles on modified nickel foam (AgNPs/NF) and indium tin oxide (AgNPs/ITO) by an ion-implantation method. NF served as both the substrate of the three-dimensional network structure and one of the catalysts. The working electrodes were followed by casting Nafion (N-AgNPs/NF and N-AgNPs/ITO) to protect the AgNPs on the electrode surface. The N-AgNPs/NF electrode was used for the electrocatalytic oxidation of methanol and exhibited remarkable catalytic activity which high stability compared with N-AgNPs/ITO. Therefore, this electrode is an attractive anode for the fabrication of methanol fuel cells.

2 Experimental section

2.1 Materials

Nickel foam (0.5 mm in thickness, ≥98% in porosity, Shenzhen Lifeixin Environment Material Co.) and ITO glass (Beijing Tsinghua Engineering Research Center of Liquid Crystal Technology) were used in this study. All reagents were of analytical grade and used without further treatment (additional purification). All solutions were prepared with triple-distilled water. All electrochemical experiments were performed at room temperature.

2.2 Preparation of the N-AgNPs/NF and N-AgNPs/ITO electrodes

The N-AgNPs/NF electrode were prepared through the following steps: (1) the NF was cut into 100 × 100 mm pieces for use as the substrate after being carefully washed by acetone, ethanol, hydrochloric acid (1 M) and triple-distilled water, then dried under nitrogen gas. (2) Silver ions with 10 keV at the fluences of 1.0×10^{17} ions cm^{-2} were implanted on the pretreated NF surface (AgNPs/NF). The preparation method of the AgNPs/ITO electrode is similar to that of previous reports.[43] All the electrodes were washed with distilled water, cut into 5 × 5 mm pieces, and dried under nitrogen gas. The Nafion solution was diluted with ethanol to 0.5 wt%, then draw 10 μL of the solution onto the electrode surface and dry at room temperature to fix AgNPs on the surface of NF. They are expressed as N-NF, N-AgNPs/NF, N-ITO and N-AgNPs/ITO.

2.3 Apparatus

The Beijing Normal University (BNU) metal vapor vacuum arc (MEVVA) implanter was used to prepare the AgNPs/NF and AgNPs/ITO electrodes. The structure and morphology of the modified electrode were observed by scanning electron microscopy (SEM) (using a Hitachi S-4800, Japan). X-ray photoelectron spectroscopy (XPS) was performed on an AXIS-Ultra instrument (Kratos, UK). Electrochemical experiments were carried out on a CHI660 electrochemical workstation (CH Instruments Inc., USA) with a conventional three-electrode setup, a bare or modified electrode (area = 25 mm^2) as the working electrode, a Ag/AgCl electrode (saturated with KCl) as the reference electrode and a platinum wire as the counter electrode.

3 Results and discussion

The SEM images of the bare NF and AgNPs/NF are shown in Fig. 1A–D, respectively. Low-magnification SEM (A and C) shows better 3D structure. After modification, the surface of the NF has no obvious change. Under high-magnification SEM, as seen in Fig. 1B, there are some sheet-shapes on the bare NF electrode surface. After ion implantation, we can observe a distinct change on the surface as a result of the formation of AgNPs (Fig. 1D). Most of the sheet faces of the bare NF disappear, as well as rougher surfaces and AgNPs are clearly observed. The AgNPs have a diameter ranging from 10 to 20 nm and are evenly distributed. Fig. S1† shows that the NF is composed of macroscopic 3D porous structure with a layer of cross-linked grid structure. The image of the N-AgNPs/NF electrode reveals its flexibility; it can be bent into a spiral or a half curl (inset in Fig. S1†). The SEM image of AgNPs/ITO is similar to that previously reported.[43]

The XPS wide-scan spectra of the bare NF and AgNPs/NF are shown in Fig. 2A. Comparing AgNPs/NF with bare NF, an obvious signal of Ag 3d is found at 374 eV besides the signals of Ni 2p, indicating that AgNPs were successfully implanted on the flexible 3D NF. Regarding to Ni, the Ni 2p spectrum of the bare NF shows a simple structure by the presence of high binding energy main peaks (Fig. 2B). Two strong satellite peaks at 855.62 eV and 873.02 eV corresponding to Ni $2p_{3/2}$ and Ni $2p_{5/2}$ of metallic NiO were observed.[44,45] However, AgNPs/NF electrode of Fig. 2B shows that the Ni $2p_{3/2}$ peak is divided into two small peaks, indicating that the introduction of Ag can change the electronic structure of Ni(II) in AgNPs/NF. The Ag 3d XPS spectrum is given in Fig. 2C, where the binding energies are at 368.12 eV for Ag $3d_{5/2}$ and 374.07 eV for Ag $3d_{3/2}$. A spin energy

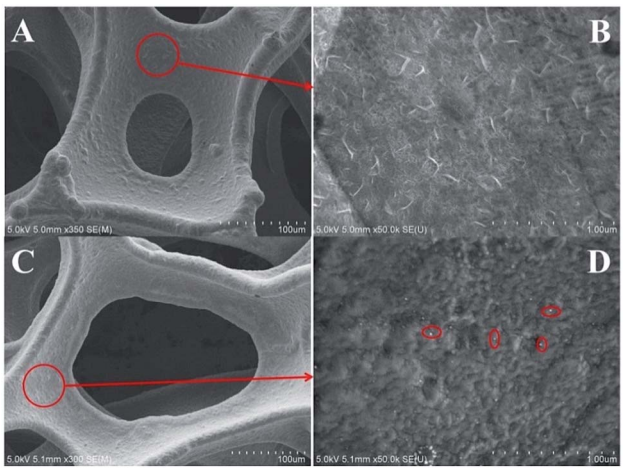

Fig. 1 Low-magnification SEM image of bare NF (A) and AgNPs/NF (C). High-magnification SEM image of bare NF (B) and AgNPs/NF (D).

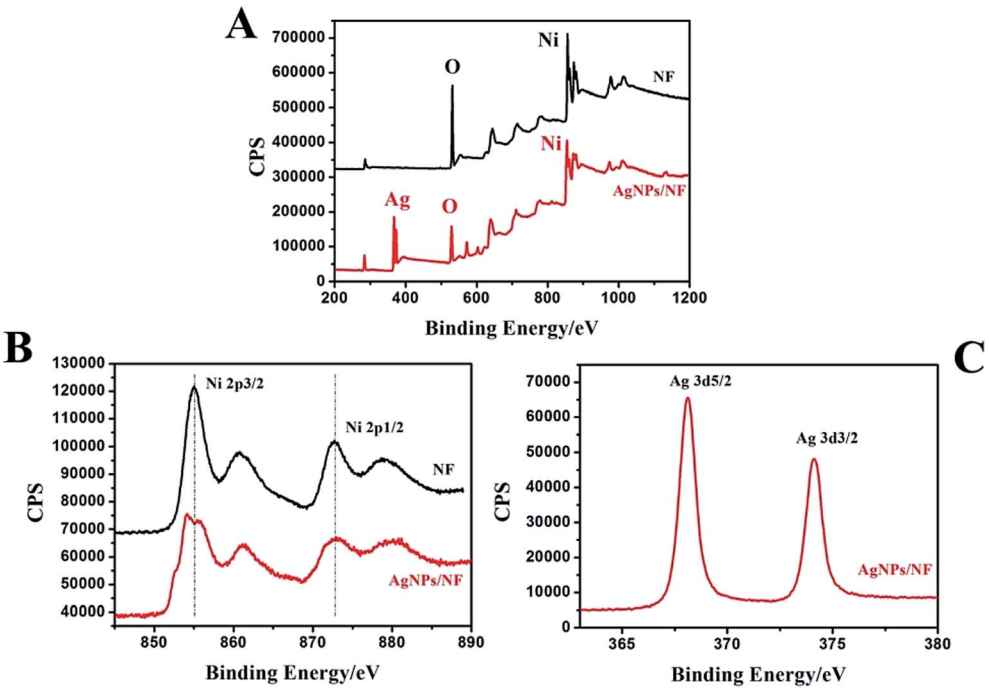

Fig. 2 XPS spectrum of the bare NF and AgNPs/NF (A). XPS spectra of the Ni 2p (B) and Ag 3d (C).

separation of 5.95 eV between Ag $3d_{5/2}$ and Ag $3d_{3/2}$ is attributed to formation of the zero valence metallic state.[46,47]

Electrochemical impedance spectroscopy (EIS) is also an efficient tool for studying the interface properties of surface-modified electrodes. The charge-transfer resistance at electrode surface is equal to the semicircle diameter of EIS and can be used to describe the interface properties of the electrode. Thus, the capability of electron transfer of different electrodes was further investigated by EIS experiments. Fig. 3 shows the EIS of different modified electrodes in 0.1 M NaOH as supporting electrolyte in the frequency range swept 10^5–0.1 Hz. The AC voltage amplitude was 5 mV and the applied potential was 0.65 V. Line b and d indicated that AgNPs/NF had better electrical conductivity than single NF. This reduced electron transfer resistance of AgNPs/NF is a result of the metal/metal interface created in dendritic Ag and Ni. A new electron transfer pathway was created by placing Ag and Ni in direct contact with each other. The electrical conductivity of the electrodes was further improved when the electrode was coated with Nafion. This result indicated that the Nafion layer on the surface of the electrode formed a barrier for electron-transfer and that AgNPs/NF was an excellent electrical conducting material that accelerated electron transfer.

CV is a significant method to demonstrate electrochemical properties of the modified electrode. Fig. 4 shows the CV of the N-NF (a) and N-AgNPs/NF (b) electrodes in 0.1 M NaOH ranging from 0.0 to 1.0 V. The electrodes had scanned 30 cycles in 0.1 M NaOH ranging from 1.0 to 1.5 V. In Fig. 4 curve a reveals the

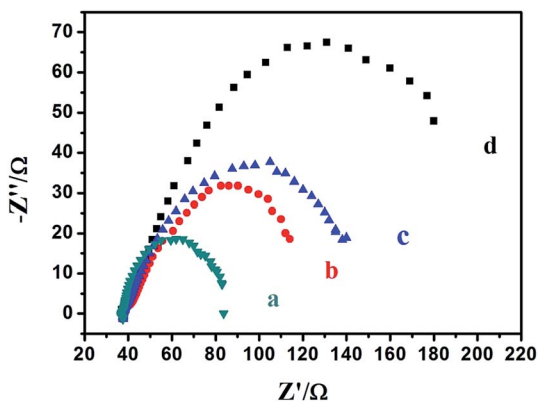

Fig. 3 EIS plots of AgNPs/NF (a), N-AgNPs/NF (b), NF (c) and N-NF (d) in 0.1 M NaOH.

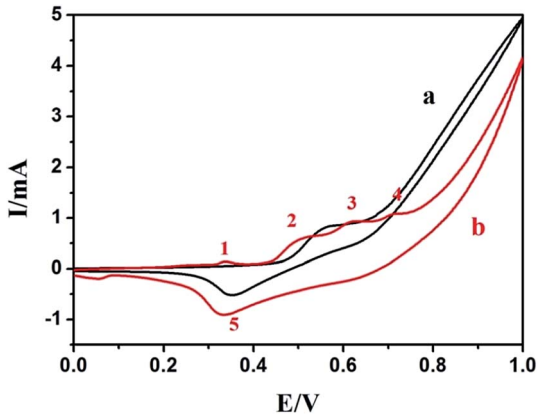

Fig. 4 The CV of the N-NF (a) and the N-AgNPs/NF (b) in 0.1 M NaOH at a scan rate of 100 mV s^{-1}.

redox peak at 0.561 V and 0.354 V which correspond to the Ni^{2+}/Ni^{3+} redox couples,[48–50] as shown in eqn (1) and (2):

$$Ni + 2OH^- \rightarrow 2Ni(OH)_2 + e^- \quad (1)$$

$$Ni(OH)_2 + OH^- \rightleftharpoons NiOOH + H_2O + e^- \quad (2)$$

Fig. S2† shows the CVs of the bare N-ITO (a) and the N-AgNPs/ITO (b) in 0.1 M NaOH. No peak was found on the bare N-ITO as shown in Fig. S2† (curve a). In contrast, the electrochemical behavior of AgNPs in alkaline solution is complex (Fig. S2† curve b). The first oxidation peak has been assigned to the oxidation of Ag(0) to Ag(I). The second oxidation peak was attributed to the oxidation of Ag(I) to Ag(II). On the cathodic sweep, signals were assigned to the reduction of Ag(II) to Ag(I) at the higher potential and the reduction of Ag(I) to Ag(0) at the lower potential.[43,51,52]

Compared with the CV of the N-AgNPs/NF (Fig. 4, curve b) and CV N-AgNPs/ITO (Fig. S2,† curve b) in 0.1 M NaOH, we suggested that the first weak oxidative current peak 1 (0.338 V) was ascribed to the oxidation of Ag(0) to Ag(I), oxidative current peak 2 (0.515 V) and peak 3 (0.617 V) were attributed to $Ni(OH)_2$/γ-NiOOH and $Ni(OH)_2$/β-NiOOH, respectively,[53–55] as shown in eqn (3) and (4). It is because of the addition of silver nanoparticles.

$$Ni(OH)_2 + OH^- \rightleftharpoons \gamma\text{-}NiOOH + H_2O + e^- \quad (3)$$

$$Ni(OH)_2 + OH^- \rightleftharpoons \beta\text{-}NiOOH + H_2O + e^- \quad (4)$$

The oxidative current peak 4 (0.707 V) is ascribed to the oxidation of Ag(I) to Ag(II). The reductive current peak observed at approximately 0.332 V (peak 5) has been described as the cathodic peak current of γ-NiOOH and β-NiOOH to $Ni(OH)_2$, while the weak peak observed at approximately 0.054 V could ascribe to the other cathodic peak current of Ag(I) to Ag(0). Compared with N-NF and N-AgNPs/ITO, N-AgNPs/ITO showed a slightly positive potential, which might be ascribed to the different over-potentials of the electrochemical reactions on different modified electrode surfaces and the metal Ag and Ni influence with each other.

Using the Randles–Ševčik equation, the electrochemically active area was found using the relationship between the peak currents and the scan rates:

$$i_p = 2.69 \times 10^5 n^{3/2} A D_0^{1/2} v^{1/2} C_0$$

where n is the number of electrons transferred, A is the effective area of the AgNPs/NF electrode, D_0 is the diffusion coefficient of the rate-limiting proton, v is the scan rate and C_0 is the concentration of $[Fe(CN)_6]^{3-/4-}$. The average slope of i_p against $v^{1/2}$ is shown in Fig. S3.† The area A is thus calculated to be 4.35×10^4 cm^2, which is much higher than the geometric area 25 mm^2.

Electrocatalytic property of nanostructured N-AgNPs/NF (electrode for the oxidation of methanol was investigated by cyclic voltammetry and compared with N-NF and N-AgNPs/ITO electrode. Herein, the AgNPs on ITO substrate was prepared in the same manner with that on NF substrate. Fig. 5A shows the

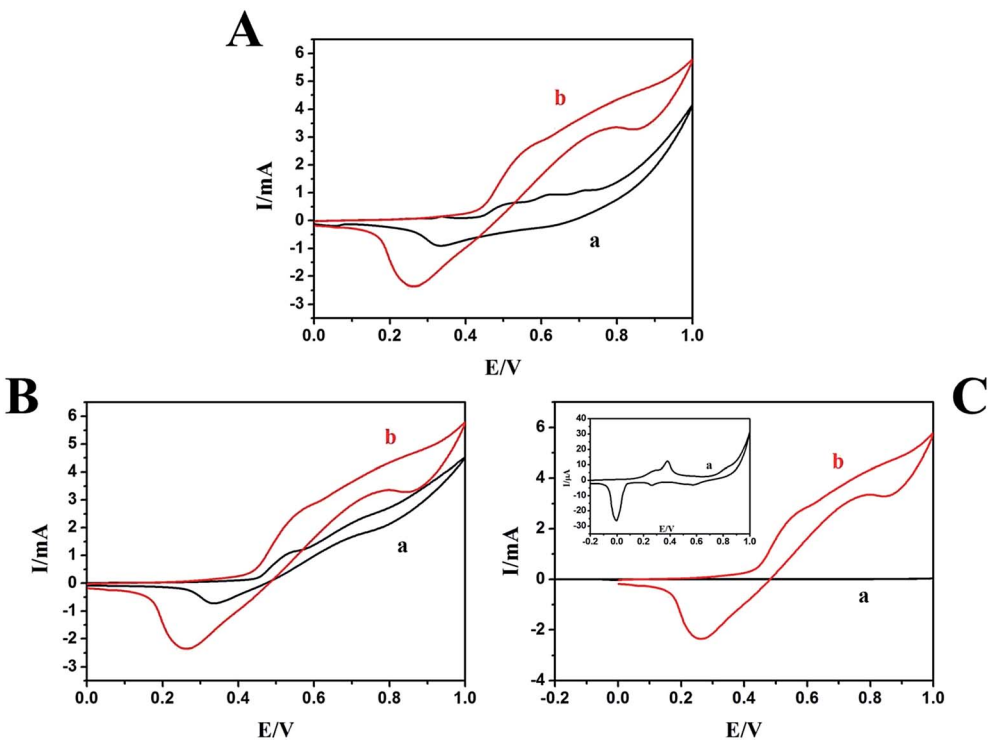

Fig. 5 (A) The CV of the N-AgNPs/NF in the absence (a) and presence (b) of 0.1 M methanol in 0.1 M NaOH. (B) The CV of the N-NF (a), N-AgNPs/NF (b) in 0.1 M NaOH with 0.1 M methanol. (C) The CV of the N-AgNPs/ITO (a) and N-AgNPs/NF (b) in the presence of 0.1 M methanol in 0.1 M NaOH. Inset: large image of the CV of the N-AgNPs/ITO in the presence of 0.1 M methanol in 0.1 M NaOH. Scan rate: 100 mV s^{-1}.

CV of the N-AgNPs/NF electrode in the absence (a) and presence (b) of 0.1 M methanol in 0.1 M NaOH. The electrocatalytic oxidation of methanol on the N-AgNPs/NF electrode is clearly observed. This is observed in curve b by two oxidation processes that are related to the electrocatalytic oxidation of methanol. During the forward sweep, there is a rapid increase in current at potentials over 0.440 V. This is due to electrocatalytic oxidation of adsorbed methanol species by Ag(I) and NiOOH. According to the CV results and previous reports,[56–60] the associated reactions are presented by eqn (5)–(7). Compared with the N-NF electrocatalytic oxidation of methanol (Fig. 5B, curve a), on the backward sweep, the irreversible oxidation current peak appears at 0.790 V. It is due to oxidation of previously adsorbed oxidizable intermediates (8).

$$\beta\text{-NiOOH} + \text{methanol} \rightarrow \text{Ni(OH)}_2 + \text{product} + e^- \quad (5)$$

$$\gamma\text{-NiOOH} + \text{methanol} \rightarrow \text{Ni(OH)}_2 + \text{product} + e^- \quad (6)$$

$$\text{Ag(I)} + \text{methanol} \rightarrow \text{Ag(I)–methanol}_{(\text{intermediate})} \quad (7)$$

$$\text{Ag(II)} + \text{Ag(I)–methanol}_{(\text{intermediate})} \rightarrow \text{Ag(I)} + \text{product} + e^- \quad (8)$$

Fig. S4† shows the CV of the N-ITO (a) and N-AgNPs/ITO (c) in the presence of 0.1 M methanol, the N-AgNPs/ITO (b) in the absence of 0.1 M methanol in 0.1 M NaOH. We do not find any peaks on the bare N-ITO electrode in the presence of 0.1 M methanol (curve a), and curve c shows a slight increase in current. The N-AgNPs/NF electrode exhibited excellent electrocatalytic activity towards the oxidation of methanol compared with the N-NF (Fig. 5B curve a) and N-AgNPs/ITO (Fig. 5C curve a) electrodes. Based on this evidence, electrocatalytic oxidation of methanol on N-AgNPs/NF seems to be certainly *via* a possible mechanism presented in Scheme 1.

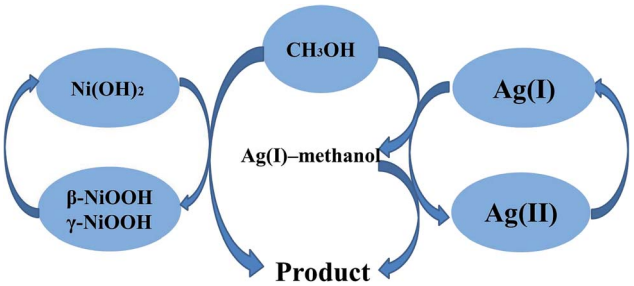

Scheme 1 Representative schematic of the mechanism of methanol electrocatalytic oxidation at the surface of N-AgNPs/NF.

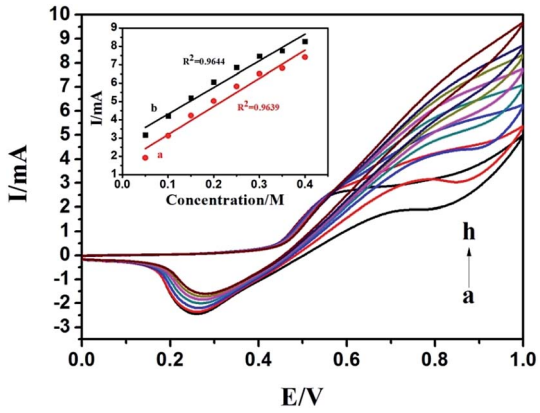

Fig. 7 The CV of the different concentrations 0.05 (a), 0.1 (b), 0.15 (c), 0.2 (d), 0.25 (e), 0.3 (f), 0.35 (g) and 0.4 (h) M of methanol in 0.1 M NaOH solution on the N-AgNPs/NF electrode. Inset: the concentrations *versus* oxidation peak (forward and backward) currents. Scan rate: 100 mV s^{-1}.

The enhanced electrochemical activity of N-AgNPs/NF can be explained as follow:

(a) The presence of AgNPs provides a larger specific surface area than NF. This is consistent with SEM results.

(b) The addition of AgNPs causes the NF to produce the β-NiOOH substance in NaOH solution. It has been reported that β-NiOOH phase enhances the oxidation of organic molecules.[61]

(c) The ion-implantation method effectively protects AgNPs from atmospheric oxidation.

(d) The 3D porous frameworks of NF can offer beneficial features for electron transfer and electrolyte diffusion.

A electro-catalytic performance comparison between AgNPs/NF and the other reported silver and nickel metals catalysts for methanol electro-catalysis in alkaline media is listed in Table

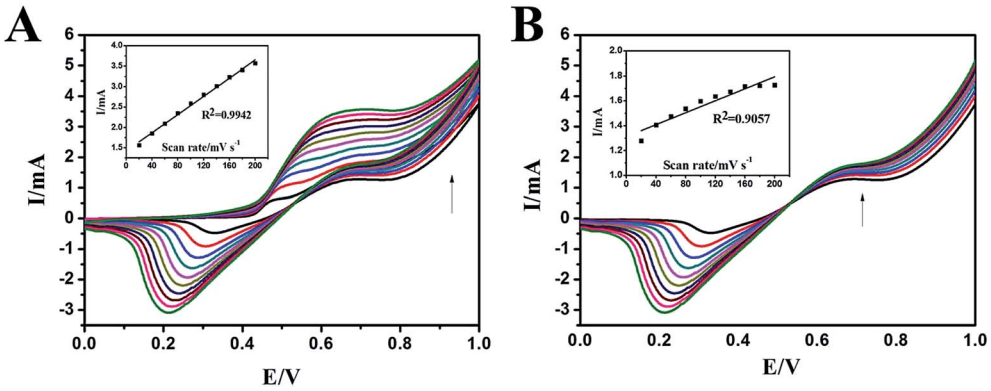

Fig. 6 (A) The CV of the N-AgNPs/NF in the presence of 0.05 M methanol in 0.1 M NaOH at various scan rates from 20 to 200 mV s^{-1} (from the inner to the outer). (B) Large image of backward oxidation peak *versus* scan rates. Inset: the oxidation peak *versus* scan rates.

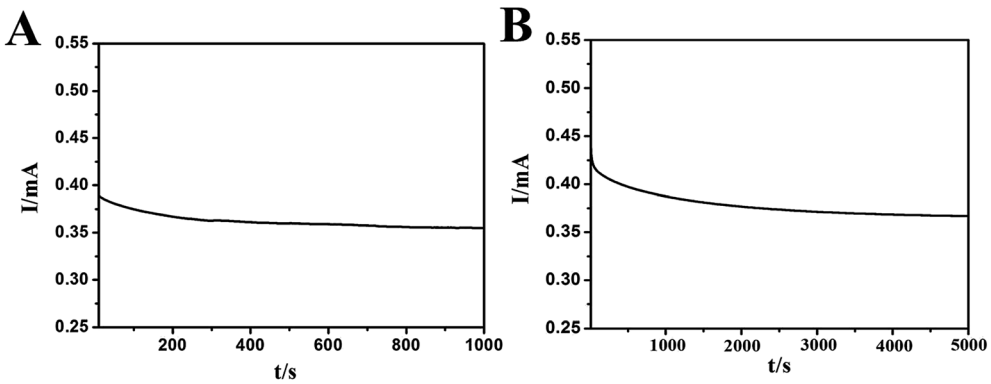

Fig. 8 Chronoamperometric responses of the N-AgNPs/NF electrode in 0.1 M NaOH towards 0.1 M methanol for 1000 s (A) and 5000 s (B).

S1,† from which the modified electrode AgNPs/NF outperforms of other electrode which are modified by Ag or Ni or di-metals.

The effect of scan rate on the electrocatalytic oxidation of methanol on the N-AgNPs/NF electrode was investigated further and reported in Fig. 6. The anodic peak in the forward sweep current increase with the scan rates, indicating that the electrochemical reaction kinetics are surface-controlled (inset, Fig. 6A). During the backward sweep, the peak currents increase slowly with the scan rate and any increase in the scan rate caused an proportional linear enhancement of the oxidation current (inset, Fig. 6B). At the second oxidation process, the electrocatalytic oxidation of Ag(I)–methanol$_{(intermediate)}$ does not have adequate reaction time with increasing the scan rate. This result shows that the mechanism which the N-AgNPs/NF electrode electrocatalytic oxidation of methanol (eqn (1)–(4)) is reasonable.

Fig. 7 presents the effect of methanol concentration on the electrocatalytic oxidation current at the N-AgNPs/NF electrode. As shown in this figure, when the concentrations are excessive, the oxidation peak currents increase. The oxidation current in the forward sweep was proportional to the concentration of methanol (Fig. 7, inset curve b). Moreover, any increase in the concentration of methanol caused a proportional linear enhancement of the oxidation current in the backward sweep (Fig. 7, inset curve a). The electrocatalytic oxidation of methanol occurs not only in the anodic half-cycle but also continues in the initial stage of the cathodic half-cycle.

Fig. 8A shows the chronoamperometric curves of the N-AgNPs/NF electrode in a 0.1 M NaOH solution with 0.1 M methanol at a constant potential of 0.80 V *versus* the Ag/AgCl reference electrode for 1000 s. This result suggests the N-AgNPs/NF electrode has a good stability during the brief oxidation of methanol. Fig. 8B displays the results of a control experiment: after approximately 2000 s of continuous operation at 0.80 V, the current density of the N-AgNPs/NF electrode reached a steady state until 5000 s. The excellent long-term stability of this electrode further implies that ion-implanted AgNPs onto the surface of NF may be a good alternative catalyst for use in direct methanol fuel cells. The proposed modified electrode was stored in air at ambient conditions and its sensitivity was checked every week. The current response was 92% of its initial value after 30 days.

4 Conclusion

In the present study, AgNPs were prepared on NF electrode-coated Nafion membranes using an ion-implantation method. The N-AgNPs/NF electrode showed excellent electrocatalytic activity for the oxidation of methanol compared with the N-AgNPs/ITO electrode. Beneficial electrocatalytic activity due to the interplay between support and AgNPs was measured. The 3D porous frameworks of NF can offer beneficial features for electron transfer and electrolyte diffusion. Meanwhile, the ion-implantation method effectively protects AgNPs from atmospheric oxidation. The N-AgNPs/NF electrode showed high stability, making it an attractive anode for the fabrication of direct methanol fuel cells (DMFCs).

Conflicts of interest

There are no conflicts to declare.

Acknowledgements

This research was supported by the Fundamental Research Funds for the Central Universities, China Scholarship Council and the National Natural Science Foundation of China (Grant No. 20873012).

References

1 S. Bauer, *Nat. Mater.*, 2013, **12**, 871–872.
2 H. Nishide and K. Oyaizu, *Science*, 2008, **319**, 737–738.
3 C. Meng, C. Liu, L. Chen, C. Hu and S. Fan, *Nano Lett.*, 2010, **10**, 4025–4031.
4 S. Park and S. Jayaraman, *MRS Bull.*, 2003, **28**, 585–591.
5 D. P. Martin and S. F. Williams, *Biochem. Eng. J.*, 2003, **16**, 97–105.
6 Q.-q. Xiong, J.-p. Tu, X.-h. Xia, X.-y. Zhao, C.-d. Gu and X.-l. Wang, *Nanoscale*, 2013, **5**, 7906–7912.
7 P. Yang, X. Xiao, Y. Li, Y. Ding, P. Qiang, X. Tan, W. Mai, Z. Lin, W. Wu and T. Li, *ACS Nano*, 2013, **7**, 2617–2626.
8 G. Nagaraju, G. S. R. Raju, Y. H. Ko and J. S. Yu, *Nanoscale*, 2016, **8**, 812–825.

9 X. Xie, M. Pasta, L. Hu, Y. Yang, J. McDonough, J. Cha, C. S. Criddle and Y. Cui, *Energy Environ. Sci.*, 2011, **4**, 1293–1297.
10 X. Xie, L. Hu, M. Pasta, G. F. Wells, D. Kong, C. S. Criddle and Y. Cui, *Nano Lett.*, 2010, **11**, 291–296.
11 H. Gao, F. Xiao, C. B. Ching and H. Duan, *ACS Appl. Mater. Interfaces*, 2012, **4**, 7020–7026.
12 X. Zhang, L. Gong, K. Liu, Y. Cao, X. Xiao, W. Sun, X. Hu, Y. Gao, J. Chen and J. Zhou, *Adv. Mater.*, 2010, **22**, 5292–5296.
13 Y. Fu, W. Su, T. Wang and J. Hu, *J. Electrochem. Soc.*, 2016, **163**, B107–B112.
14 S. Langlois and F. Coeuret, *J. Appl. Electrochem.*, 1989, **19**, 43–50.
15 S. Langlois and F. Coeuret, *J. Appl. Electrochem.*, 1989, **19**, 51–60.
16 Y. Jiang, J. Chen, J. Zhang, A. Li, Y. Zeng, F. Zhou, G. Wang and R. Wan, *RSC Adv.*, 2016, **6**, 13207–13216.
17 X. Yang, Z. Lin, J. Zheng, Y. Huang, B. Chen, Y. Mai and X. Feng, *Nanoscale*, 2016, **8**, 8650–8657.
18 Y. Cheng, Y. Liu, D. Cao, G. Wang and Y. Gao, *J. Power Sources*, 2011, **196**, 3124–3128.
19 H. Kim, K. Kim, E. Song and J. Song, *Appl. Therm. Eng.*, 2015, **89**, 600–608.
20 B. G. Gang, W. Jung and S. Kwon, *Int. J. Hydrogen Energy*, 2016, **41**, 524–533.
21 P. Ganesan, A. Sivanantham and S. Shanmugam, *J. Mater. Chem. A*, 2016, **4**, 16349–16402.
22 X. Wang, W. Li, D. Xiong and L. Liu, *J. Mater. Chem. A*, 2016, **4**, 5639–5646.
23 R. Jin, G. Li, Z. Zhang, L.-X. Yang and G. Chen, *Electrochim. Acta*, 2015, **173**, 458–464.
24 Y. Li, Y. Tao, D. Ke, Y. Ma and S. Han, *Appl. Surf. Sci.*, 2015, **357**, 1714–1719.
25 S. Qiu, S. Xu, G. Li and J. Yang, *Materials*, 2016, **9**, 457–469.
26 B. Yang, G. Yu and D. Shuai, *Chemosphere*, 2007, **67**, 1361–1367.
27 A. Panáček, R. Prucek, J. Hrbáč, T. j. Nevečná, J. Šteffková, R. Zbořil and L. Kvítek, *Chem. Mater.*, 2014, **26**, 1332–1339.
28 S. Singha, D. Kim, H. Seo, S. W. Cho and K. H. Ahn, *Chem. Soc. Rev.*, 2015, **44**, 4367–4399.
29 N. Aliakbar, A. G. Roghayeh, N. Seyed Ali, A. Majidreza, H. Sharareh, A. Masoud, S. Shahla, H. Mehran, A. Mahdi and J. Fereshteh, *International Journal of Basic Science in Medicine*, 2016, **1**, 25–28.
30 N. Atar, T. Eren, B. Demirdögen, M. L. Yola and M. O. Çağlayan, *Ionics*, 2015, **21**, 2285–2293.
31 L. Li, M. Chen, G. Huang, N. Yang, L. Zhang, H. Wang, Y. Liu, W. Wang and J. Gao, *J. Power Sources*, 2014, **263**, 13–21.
32 K. Han, P. Miao, H. Tong, T. Liu, W. Cheng, X. Zhu and Y. Tang, *Appl. Phys. Lett.*, 2014, **104**, 053101–053105.
33 A. Desireddy, B. E. Conn, J. Guo, B. Yoon, R. N. Barnett, B. M. Monahan, K. Kirschbaum, W. P. Griffith, R. L. Whetten and U. Landman, *Nature*, 2013, **501**, 399–402.
34 W. Lian, S. Liu, J. Yu, J. Li, M. Cui, W. Xu and J. Huang, *Biosens. Bioelectron.*, 2013, **44**, 70–76.
35 Y. Li, P. Zhang, Z. Ouyang, M. Zhang, Z. Lin, J. Li, Z. Su and G. Wei, *Adv. Funct. Mater.*, 2016, **26**, 2122–2134.
36 D. Cao, Y. Gao, G. Wang, R. Miao and Y. Liu, *Int. J. Hydrogen Energy*, 2010, **35**, 807–813.
37 Y. Cheng, Y. Liu, D. Cao, G. Wang and Y. Gao, *J. Power Sources*, 2011, **196**, 3124–3128.
38 H. He, H. Liu, F. Liu and K. Zhou, *Surf. Coat. Technol.*, 2006, **201**, 958–964.
39 W. Yang, S. Yang, W. Sun, G. Sun and Q. Xin, *Electrochim. Acta*, 2006, **52**, 9–14.
40 T. Iwasita, *Electrochim. Acta*, 2002, **47**, 3663–3674.
41 X. Zhao, M. Yin, L. Ma, L. Liang, C. Liu, J. Liao, T. Lu and W. Xing, *Energy Environ. Sci.*, 2011, **4**, 2736–2753.
42 X. Niu, H. Zhao and M. Lan, *J. Power Sources*, 2016, **306**, 361–368.
43 Y. Yu, M. Jia, H. Tian and J. Hu, *J. Power Sources*, 2014, **267**, 123–127.
44 I.-M. Chan and F. C. Hong, *Thin Solid Films*, 2004, **450**, 304–311.
45 A. Mansour, *Surf. Sci. Spectra*, 1994, **3**, 231–238.
46 I. Lopez-Salido, D. C. Lim and Y. D. Kim, *Surf. Sci.*, 2005, **588**, 6–18.
47 N. Atar, T. Eren, M. L. Yola, H. Gerengi and S. Wan, *Ionics*, 2015, **21**, 3185–3192.
48 Y. Yu, W. Su, M. Yuan, Y. Fu and J. Hu, *J. Power Sources*, 2015, **286**, 130–135.
49 M. Vuković, *J. Appl. Electrochem.*, 1994, **24**, 878–882.
50 S. Medway, C. Lucas, A. Kowal, R. Nichols and D. Johnson, *J. Electroanal. Chem.*, 2006, **587**, 172–181.
51 M. Jia, T. Wang, F. Liang and J. Hu, *Electroanalysis*, 2012, **24**, 1864–1868.
52 H. Quan, S.-U. Park and J. Park, *Electrochim. Acta*, 2010, **55**, 2232–2237.
53 G. Hu, C. Li and H. Gong, *J. Power Sources*, 2010, **195**, 6977–6981.
54 N. Bagheri, A. Aghaei, N. Vlachopoulos, M. Skunik-Nuckowska, P. J. Kulesza, L. Häggman, G. Boschloo and A. Hagfeld, *Electrochim. Acta*, 2016, **194**, 480–488.
55 M. Gong and H. Dai, *Nano Res.*, 2015, **8**, 23–39.
56 D. J. Guo and H. L. Li, *Carbon*, 2005, **43**, 1259–1264.
57 M. Avramov-Ivić, V. Jovanović, G. Vlajnić and J. Popić, *J. Electroanal. Chem.*, 1997, **423**, 119–124.
58 A. El-Shafei, *J. Electroanal. Chem.*, 1999, **471**, 89–95.
59 G. S. Ferdowsi, S. Seyedsadjadi and A. Ghaffarinejad, *J. Nanostruct. Chem.*, 2015, **5**, 17–23.
60 G.-P. Jin, R. Baron, N. V. Rees, L. Xiao and R. G. Compton, *New J. Chem.*, 2009, **33**, 107–111.
61 R. H. Tammam, A. M. Fekry and M. M. Saleh, *Int. J. Hydrogen Energy*, 2015, **40**, 275–283.